HHS Public Access

Author manuscript

J Immunol. Author manuscript; available in PMC 2016 May 15.

Published in final edited form as:

J Immunol. 2015 May 15; 194(10): 4846–4859. doi:10.4049/jimmunol.1402295.

Obesity increases mortality and modulates the lung metabolome during pandemic H1N1 influenza virus infection in mice[1]

J. Justin Milner[*], **Jenny Rebeles**[*], **Suraj Dhungana**[†], **Delisha A. Stewart**[†], **Susan C.J. Sumner**[†], **Matthew H. Meyers**[*], **Peter Mancuso**[‡], and **Melinda A. Beck**[*]

[*]Department of Nutrition, Gillings School of Global Public Health, University of North Carolina at Chapel Hill, Chapel Hill, NC, USA

[†]Systems and Translational Science Center, RTI International, Research Triangle Park, NC

[‡]Department of Environmental Health Sciences, The University of Michigan, Ann Arbor, MI, United States

Abstract

Obese individuals are at greater risk for hospitalization and death from infection with the 2009 pandemic H1N1 influenza virus (pH1N1). In this study, diet-induced and genetic-induced obese mouse models were utilized to uncover potential mechanisms by which obesity increases pH1N1 severity. High fat diet-induced and genetic-induced obese mice exhibited greater pH1N1 mortality, lung inflammatory responses and excess lung damage despite similar levels of viral burden compared with lean control mice. Further, obese mice had fewer bronchoalveolar macrophages and regulatory T cells during infection. Obesity is inherently a metabolic disease, and metabolic profiling has found widespread usage in metabolic and infectious disease models for identifying biomarkers and enhancing understanding of complex mechanisms of disease. To further characterize the consequences of obesity on pH1N1 infection responses, we performed global liquid chromatography-mass spectrometry metabolic profiling of lung tissue and urine. An array of metabolites were perturbed by obesity both prior to and during infection. Uncovered metabolic signatures were used to identify changes in metabolic pathways that were differentially altered in the lungs of obese mice such as fatty acid, phospholipid, and nucleotide metabolism. Taken together, obesity induces distinct alterations in the lung metabolome, perhaps contributing to aberrant pH1N1 immune responses.

Introduction

The triple reassortant H1N1 influenza virus (pH1N1) caused the first pandemic of the 21st century in 2009, and this strain continues to circulate and contribute to seasonal influenza epidemics globally (1, 2). Although infection with the pH1N1 strain typically results in relatively mild, uncomplicated symptoms, a number of epidemiological investigations have identified obesity as an independent risk factor for hospitalization and death to pH1N1 (3–

Address correspondence and reprint requests to Dr. Melinda A. Beck, Department of Nutrition, Gillings School of Global Public Health 2303 MHRC, CB No. 7461, University of North Carolina at Chapel Hill, Chapel Hill, NC 27599-7461. T:919-966-6809, F: 919-843-0776, melinda_beck@unc.edu.

6). More than 500 million individuals are obese (body mass index ≥30kg/m^2) globally (7), and thus, understanding the mechanisms by which excess adiposity drives greater pH1N1 infection severity is critical for solving this public health threat.

Similar to humans, obese mice are also more susceptible to influenza infection mortality compared with lean controls (8, 9). Several reports have demonstrated that obesity alters inflammatory and pathological responses in the lung during influenza infection in mice, but the underlying mechanisms causing these aberrant immune responses and ultimately death remain unclear (10–15). Excess accumulation of adipose tissue triggers metabolic and physiologic perturbations such as insulin resistance, hyperleptinemia, oxidative stress, low-grade chronic inflammation and alterations in a variety of circulating nutrients and hormones, all of which could potentially affect influenza immunity and disease severity (8, 16).

Although our understanding of host immune responses to influenza virus infection *in vitro* and *in vivo* are well established, much remains unknown regarding the mechanisms in which perturbations in systemic metabolism may impact influenza immune responses and infection mortality. This is pertinent because not only is obesity a highly prevalent metabolic disease, but other risk factors for severe influenza infections, such as heart disease, diabetes, pregnancy and aging (17, 18) are also associated with distinct cellular and systemic metabolic complications (16, 19, 20). Metabolic profiling has been useful for identifying biomarkers or uncovering complex mechanisms in a number of metabolic diseases such as cardiovascular disease, type II diabetes and obesity (21, 22). Further, application of this methodology to infectious diseases models continues to gain momentum, facilitating greater understanding of the complex interactions between pathogen and host and identifying prognostic or diagnostic biomarkers/metabolic signatures unique to certain disease states and stages (23–26). Although lipidomics has recently proven useful in identifying lipid metabolites that have antiviral effects (27) or serve as influenza biomarkers (28), metabolomics has only been applied to a few influenza models *in vitro* (29, 30) or *in vivo* (26, 31). Relatively little is known regarding the consequences of influenza virus infection on the global lung metabolome (at the site of infection) or how altered systemic metabolism (e.g. obesity) may impact influenza pathogenesis and metabolic processes in the lung.

In this study we used two models of obesity, diet- and genetic-induced, providing a robust characterization of the immunological and metabolic consequences of obesity during pH1N1 infection. High fat diet (HFD)-induced and genetic-induced obese mice exhibited greater pH1N1 mortality, as well as elevated lung inflammatory responses and excess lung damage, despite similar viral titers compared with lean control mice. Additionally, both models of obesity exhibited distinct alterations in immune cell populations, such as fewer macrophages and regulatory T cells (Tregs) in the airways. We also demonstrated that the lung metabolome was differentially altered by obesity during influenza virus infection. Further, UPLC-MS profiling successfully distinguished urine samples from infected lean and obese mice as early as 2 days post infection (dpi), and the urine from infected obese mice reflected alterations in a diverse number of metabolic pathways. Pathway enrichment analyses, based on the uncovered metabolic signatures in lung tissue and urine, revealed differentially regulated metabolic processes that perhaps may be contributing to greater pH1N1 severity in

obese mice, such as fatty acid, phospholipid and nucleotide metabolism. Taken together, this report provides an in-depth analysis of the immunological and metabolic consequences of obesity during influenza virus infection.

Materials and methods

Mice and diets

Diet-induced obesity was achieved by maintaining weanling, male C57BL6/J mice (obtained from The Jackson Laboratory, Bar Harbor, ME) on a high fat diet (HFD, 60% kcal fat, Research Diets D12492, New Brunswick, NJ), and lean mice were maintained on a low fat diet (LFD, 10% kcal fat, Research Diets D12450B) or a standard chow diet (CD, 14% kcal fat, ProLab RMH 3000, LabDiet, St. Louis, MO) for 14–16 wks. The HFD and LFD are nutritionally defined and contain purified ingredients. The HFD and LFD are nutritionally matched except for fat content and carbohydrate content (70% kcal in LFD and 20% kcal in HFD provided by carbohydrates). For the CD, calories are derived from 26% protein, 14% fat, and 60% carbohydrate.

Genetically-induced obesity was achieved by crossing fully floxed leptin receptor mice on a C57BL6/J background (generously provided by Dr. Alyssa Hasty) with C57BL/6J-Tg(Nkx2-1-cre)2S and/J mice purchased from the Jackson Laboratory. Fully floxed mice expressing the Cre transgene under control of the Nkx2.1 promoter ($LepR^{H-/-}$), lack leptin receptor signaling in hypothalamic neurons ($LepR^{H-/-}$) and become obese due to hyperphagia (32). Heterozygous breeding using $LepR^{H+/-}$ and $LepR^{Hfl/fl}$ mice was necessary since homozygous $LepR^{H-/-}$ mice do not produce offspring (32). Mice were genotyped as previously described (32) and housed in isolation cubicles at UNC, which is fully accredited by the American Association for Accreditation of Laboratory Animal Care. All procedures involving the use of mice were fully approved by the UNC Institutional Animal Care and Use Committee.

Influenza virus infection and viral titers

Influenza A/California/04/2009 (BEI Resources, Bethesda, MD) was propagated in embryonated hen's eggs and titered via a modified 50% tissue culture infective dose ($TCID_{50}$) using hemagglutination as an endpoint and evaluated by the method of Reed and Muench (33) as previously described (8, 12). Mice were lightly anesthetized via isoflurane inhalation and were infected intranasally with 0.05mL of 5.8×10^2 $TCID_{50}$ or 1.3×10^3 $TCID_{50}$ as described in Figure Legends. For diet-induced obese mouse models, mice were infected at 17–19 wks old. For $LepR^{Hfl/fl}$ and $LepR^{H-/-}$ mice were infected at 12–25 wks of age ($LepRH^{fl/fl}$ and $LepR^{H-/-}$ were age matched). For influenza viral titers of infected mice, bronchoalveolar lavage fluid (BALF) was titered via a modified $TCID_{50}$ in replicates of four.

Serum and BALF measurements

BALF was obtained as previously described (14). ELISA kits were used to measure serum leptin (Invitrogen, Carlsbad, CA), triacylglycerol (TAG, Pointe Scientific, Canton, MI), insulin (Uppsala, Sweden) and adiponectin (Abcam, Cambridge, UK). Blood glucose was

measured via a 6h or 14h fast as described in figure legends. Further, BALF albumin was measured with the Mouse Albumin ELISA Kit (Genway Biotech, Inc., San Diego, CA). Total protein in BALF was measured via standard BCA assay (BCA kit, Sigma-Aldrich, St Louis, MO). BALF cytokines (IL-4, IFN-γ, MCP-1, RANTES, KC, IL-17A, IL-10 and TNF-α) were measured using a BioRad Bio-Plex assay (Hercules, CA) per manufacturer's instructions. IL-4 was not measureable above the lower limit of the assay.

Lung Histopathology

The left lobe of the lung was inflated and fixed with 10% neutral buffered formalin. Fixed lung tissue was embedded in paraffin and processed for H&E staining by the UNC Animal Histopathology Core Facility. The extent of lung immune cell infiltration was scored blindly according to a scale from 0 to 4: 0, no inflammation; 1, mild influx of inflammatory cells; 2, increased inflammation with ~25–50% of the total lung involved; 3, severe inflammation involving 50–75% of the lung; and 4, almost all lung tissue contains inflammatory infiltrate (12, 14)

Flow Cytometry

Lung, mediastinal lymph nodes (mLN) and BAL cells were stained for flow cytometry as previously described (14). For staining of BAL cells from uninfected mice, BAL samples were pooled from 2 individual mice to obtain a sufficient number of cells (2 pooled BAL samples represents n=1). The following antibodies were used: CD4 (FITC, PE-Cy7), CD103 (PE), Foxp3 (APC), Ly6G (FITC), NK1.1 (PE-Cy7) and F4/80 (APC) from eBioscience (San Diego, CA) and CD8 (PerCP) and CD3 (APC-Cy7) from BioLegend (San Diego, CA) and CD25 (FITC) from BD Biosciences (San Jose, CA). For intracellular staining, all cells were fixed and permeabilized using the Foxp3 staining buffer kit (Ebioscience). All samples were run on a CyAn ADP Analyzer flow cytometer (Beckman Coulter, Inc., Fullerton, CA) and analyzed with FlowJo software (Treestar, Ashland, OR). All cells were analyzed by first utilizing a doublet exclusion gate followed by gating of $CD3^+$ T cells for further analysis of $CD4^+$ and $CD8^+$ T-cell populations or by gating on $CD3^-$ cells for further analysis of macrophages ($F4/80^+$), neutrophils ($Ly6G^+$) or NK cells ($NK1.1^+$).

Metabolic Profiling

Lung tissue was harvested and immediately frozen in liquid nitrogen. Urine was collected as previously described (25). To every 10 mg of lung tissue 100 μl of 50:50 acetonitrile:water was added and the tissue was homogenized using a bead beater operating at 1750 rpm. A 300 μl sample of lung homogenate was spiked with tryptophan-d_5 internal standard, lyophilized, reconstituted in 100 μl of 95:5 water:methanol, and 10 μl was injected into a SYNAPT G2 QTOF mass spectrometer coupled to an Acquity UPLC (Waters Corporation, MA) for broad spectrum metabolomics analysis. The lung metabolites were separated on a Waters Acquity BEH HSS T3 column (2.1 × 100mm, 1.8 μm particle size) operating at 50°C using a reversed-phase chromatographic method. A gradient mobile phase consisting of water with 0.1% formic acid (A) and methanol with 0.1% formic acid (B) were used as previously described (34).

Urine samples (25 μl) were diluted with acetonitrile containing tryptophan-d_5 internal standard (75 μl). A 5 μl diluted urine was injected into a SYNAPT G2 QTOF mass spectrometer coupled to an Acquity UPLC (Waters Corporation, MA) for broad spectrum metabolomics analysis. The urine metabolites were separated on a Waters Acquity BEH Amide column (2.1 × 150mm, 1.7 μm particle size) operating at 40°C using a HILIC chromatographic method. A gradient mobile phase consisting of 10 mM ammonium acetate in 95/5 Acetonitrile/H_2O with 0.1% Formic Acid (A) and 10 mM ammonium acetate in 50/50 Acetonitrile/H_2O with 0.1% Formic Acid (B) was used under the following conditions: 0–1.0 min 1% B, 1.0–12.0 min 100% B, 14.0–15.0 1% B, 15.0–19.0 1% B.

All MS data were collected over 50–1000 m/z in ESI positive and negative ion modes. Leucine enkephalin was used as the lock mass and a lock mass scan was collected every 45 sec and averaged over 3 scans to perform mass correction. Source and desolvation temperatures were set at 110 °C and 450 °C, respectively. All MS data analysis (alignment, normalization and peak picking) were performed using Progenesis QI (Waters Corporation). Multivariate analysis (PCA and OPLS-DA) of the metabolomics data was performed using SIMCA (Umetrics, Umea, Sweden) (35). Putative identification of the group differentiating metabolites was made using a database search against RTI-RCMRC's in-house exact-mass-retention-time library of standards (~500 compounds) and Human Metabolome Data Base release version 3.50 (HMDB). Pathway analysis was performed using GeneGO Metacore (Thomson Reuters).

Quantitation of lung gene expression

Total RNA was isolated from lung tissue via the TRIzol method (Invitrogen), and reverse transcription was performed with Superscript II First Strand Synthesis kit (Invitrogen) and oligo (dT) primers. Cytokine and chemokine expression were quantified using qRT-PCR as previously described (36). Gene expression levels were normalized to β-actin.

Statistical analysis

For all statistical analyses, JMP Statistical Software (SAS Institute, Cary, NC) or GraphPad (San Diego, CA) were used. For parametric data (including metabolites), statistical significance was evaluated using a two-way ANOVA or a two-tailed unpaired Student *t* test. Nonparametric data was evaluated using the Wilcoxon signed rank test or Kruskal Wallis test. Mean values were considered statistically significant at $p \leq 0.05$. The log-rank test was used to compare percent survival.

Results

Diet-induced obese mice are more susceptible to pH1N1 mortality compared with CD fed and purified LFD fed lean mice

Epidemiological evidence demonstrates that obesity increases the likelihood of severe influenza infection complications in humans (17, 37–40), and several mouse models have also confirmed this outcome (10–15, 36). Obesity exacerbates lung inflammation and pathology, alters lung immune cell populations, impairs lung healing and in some cases increases viral titers during influenza infection in mice (10–15, 36). To further investigate

the consequences of obesity on pH1N1 immunity, weanling male C57Bl6/J mice were fed a purified HFD (60% kcal fat), a purified LFD (10% kcal fat, nutritionally matched to the HFD except for fat and carbohydrate content) or a standard CD (14% kcal fat). The two low fat control diets (LFD and CD) were included because although previous studies have utilized both of these diets as controls for a HFD, they have never been directly compared to each other in the same study (10–15, 36). As expected, mice fed a HFD gained significantly more weight compared with LFD and CD fed mice (Figure 1A). Although LFD and CD mice exhibited relatively similar levels of weight gain in comparison with HFD-induced obese mice, LFD mice weighed significantly more than CD mice after 8 wks on the diet. Obesity results in metabolic perturbations, reflected by alterations in a number of circulating hormones and nutrients (16). In Figure 1B, we demonstrate that HFD fed obese mice had elevated fasting blood glucose measures compared with LFD and CD mice. Further, serum insulin was elevated in HFD mice compared with CD mice, and LFD mice exhibited a relatively intermediate concentration. Additionally, HFD mice had a greater concentration of serum triacylglycerol (TAG) and leptin but lower adiponectin levels. In summary, HFD mice exhibited prototypical characteristics of obesity, while LFD mice exhibited a somewhat intermediate phenotype compared with HFD and CD mice.

After 14–16 wks on the diet, mice were infected with 5.8×10^2 $TCID_{50}$ of the 2009 pandemic H1N1 virus, influenza A/Cal/04/09 (pH1N1). Strikingly, while no CD mice succumbed to the pH1N1 infection, 40% of LFD mice and more than 80% of HFD mice died by 10 dpi (Figure 1C). HFD fed obese mice exhibited a significantly higher mortality rate compared with both LFD and CD mice. Although it has been shown that diet-induced obese mice are more susceptible to pH1N1 mortality (10), it has never been demonstrated that LFD fed mice are also more likely to die from influenza infection compared with CD mice. Analysis of absolute weight loss and percent weight loss demonstrated that CD mice recover faster from the infection compared with HFD and LFD mice (Figures 1D/E).

Given that all CD mice survived the infection, we next tested if the discrepancy in pH1N1 mortality between the three dietary groups was maintained with a greater pH1N1 dose. All three dietary groups were infected with 1.3×10^3 $TCID_{50}$, and by 7 dpi, 83% of HFD mice died (Figure 1F) compared with 55% of LFD mice and only 33% of CD mice. Despite the increased death in all dietary groups compared with the previous lower dose, the mortality differences between the dietary groups were relatively maintained in that HFD and LFD mice were more susceptible to mortality compared with CD mice ($p<0.005$, $p=0.05$ respectively), and HFD mice trended towards increased mortality compared with LFD mice ($p=0.08$). There were no differences in total weight loss between the three groups (Figure 1G), but HFD mice displayed a significantly lower percent weight loss over the course of the infection compared with LFD and CD mice (Figure 1H), which has been reported previously (10). In summary, we show that HFD-induced obesity increases pH1N1 infection severity compared with two different lean mouse models. Given that LFD mice exhibited greater mortality than CD mice, simply changing the components of a diet (without inducing any nutritional deficiencies) can modulate influenza infection severity, and thus we cannot rule out synergistic effects of a HFD and obesity.

Diet-induced obese mice exhibit greater lung damage and inflammation during a pH1N1 infection

To assess potential mechanisms for the discrepancies in pH1N1 mortality between dietary groups, we measured the viral titers in the lung airways of CD, LFD and HFD mice infected with 5.8×10^2 $TCID_{50}$. There were no differences in viral titers among the three groups at 4 or 8 dpi (Figure 2A). While some studies report that obesity does not impact influenza titers (67,77), it has also been shown that obesity can increase pH1N1 titers (80).

We then assessed the level of cellular infiltration and lung pathology during the pH1N1 infection. HFD, LFD and CD mice exhibited similar bronchoalveolar lavage (BAL) and lung total cell numbers during the infection (Figure 2B/C). As expected, H&E stained lungs revealed that pH1N1 infection caused distinct pathological changes in the bronchioles, vessels and alveoli of all three dietary groups (Figure 2D). At 4 dpi, partial bronchiole denuding and perivascular cuffing occurred in all three dietary groups. By 8 dpi, perivascular cuffing, bronchial denuding and immune cell infiltration increased in all three dietary groups compared with the day 4 time point. Histopathology scores of total lung infiltration revealed there were no significant differences among the three dietary groups (data not shown), consistent with similar total BAL and lung cell numbers.

To assess the level of damage to the alveolar-endothelial barrier, total protein and albumin were measured in BALF from pH1N1 infected CD, LFD and HFD mice (Figure 2E/F). At 4 dpi, HFD mice exhibited a greater fold increase in BALF protein compared with LFD and CD mice (Figure 2E). Further, at 8 dpi, HFD mice displayed a greater fold increase in BALF protein compared with CD mice. Additionally, HFD mice exhibited a greater fold increase in BALF albumin compared with LFD and CD mice at 4 dpi (Figure 2F). Therefore, obesity enhances lung epithelial cell injury during pH1N1 infection despite no differences in viral burden or total leukocyte recruitment.

Cytokine and chemokine production in the lung airways of the three dietary groups was also measured via a multiplex assay to assess inflammatory responses (Figure 2G). HFD mice had elevated levels of the keratinocyte chemoattractant (KC or CXCL1) and MCP-1 compared with LFD and CD mice at 8 dpi. TNF-α was greater in HFD and CD mice at 8dpi compared with LFD mice. There were no differences in IFN-γ, IL-10, IL-17A or RANTES. Taken together, despite no differences in lung inflammatory cell infiltration and viral titers, HFD mice exhibited greater lung injury and production of inflammatory cytokines during pH1N1 infection.

HFD-induced obese mice have fewer macrophages and Tregs in the lung airways compared with lean mice

In order to gain a better understanding of the causes and consequences of greater lung injury and alterations in chemokine expression in HFD mice, the distribution of innate immune cells in the airways of pH1N1 infected CD, LFD and HFD mice was assessed. Figure 3A is a representative flow cytometry histogram for identification of macrophages, neutrophils and natural killer (NK) cells. Figure 3B represents the percentages (top) and numbers (bottom) of $F4/80^+$ macrophages, $NK1.1^+$ NK cells and $Ly6G^+$ neutrophils. Unexpectedly,

HFD mice had significantly fewer BAL macrophages at 4 dpi, trending fewer NK cell number (p=0.07), and similar numbers of neutrophils with CD mice. Although HFD mice had greater levels of KC and MCP-1 expression (neutrophil and macrophage chemokines, respectively), this did not result in greater infiltration of macrophages or neutrophils.

We then measured the distribution of $CD4^+$ and $CD8^+$ T cells in the BAL, lung and mLN of the three dietary groups. HFD mice had fewer BAL $CD4^+$ T cells at 8 dpi with no differences in $CD8^+$ T cell numbers compared with CD mice (Figure 3C/D). Given the alterations in T cell numbers detected in the lung airways, $CD4^+$ and $CD8^+$ T cell numbers were measured in lung tissue and in mLN at 4 and 8 dpi. There were no differences in lung or mLN T cell numbers between CD and HFD mice (data not shown).

$CD4^+Foxp3^+$ Tregs have been shown to curtail inflammatory responses to RSV and some influenza infection models in mice (41–43). Because we detected fewer BAL $CD4^+$ T cells in HFD mice, we also suspected fewer BAL Treg cells as well, perhaps contributing to heightened lung inflammation and damage in HFD mice. Figure 3E is a representative gating scheme for identification of BAL Tregs in CD, LFD and HFD mice. HFD mice had a significantly greater percentage of Tregs at 4 dpi (Figure 3E), and consistent with fewer $CD4^+$ T cells at 8 dpi, HFD mice had fewer Tregs at 8 dpi (Figure 3F). Additionally, the level of Treg activation via CD103 expression was measured (44), and HFD mice had fewer $CD103^+$ BAL Tregs as well (Figure 3G). Given the discrepancy in Treg number in the lung airways, Treg distribution in lung tissue and mLN were also assessed (Figure 3H/I). HFD mice had fewer Tregs at 0 and 4 dpi in the lung tissue and fewer at 8 dpi in the mLN compared with LFD mice.

Metabolic profiling distinguishes lung samples from uninfected and infected obese mice

Obesity is inherently a metabolic disease, and metabolic profiling has found widespread usage in infectious disease models for identifying biomarkers and improving our understanding of these complex diseases (23–26). Therefore, we hypothesized that metabolic profiling would not only provide a snapshot of the metabolic consequences of obesity in the lung during pH1N1 infection, but would also shed light on potential mechanisms driving greater pH1N1 severity in obese mice. Lungs were harvested from CD, LFD and HFD mice at 0, 4, and 8 dpi, and UPLC-MS metabolic profiling was performed. In Figure 4A, the orthogonal partial least squares discriminant analysis (OPLS-DA) plot shows significant separation between lung samples from uninfected CD and HFD mice. As one might expect, several metabolites were altered by the HFD and/or obesity, and a majority of these metabolites were related to lipid metabolism (involved in fatty, cholesterol or phospholipid metabolic pathways). Once infected, the HFD and CD lung metabolic profiles continued to separate (Figure 4B). An increase in differential metabolites was observed in HFD infected mice at 4 dpi, particularly in phospholipid and nucleotide metabolites (Figure 4B).

By 8 dpi, the number of metabolites significantly altered by obesity more than doubled compared with uninfected lung tissue (Figure 4C). Fatty acid and phospholipid related species comprised a majority of significantly altered metabolites in HFD mice at 8 dpi. Further several amino acid and ketone metabolites were detected at high levels in the lungs

(with (S)-3-hydroxybutyric acid detected at a 17.5x greater concentration in lungs of HFD mice, $p<0.0005$). Few of the differentially altered metabolites in uninfected HFD mice were also different at 8 dpi, indicating that the detected metabolic changes occurring in the lung during infection are not simply due to obesity or HFD feeding, but are a consequence of the infection in the HFD-induced obese mice.

Lastly, we determined if the unique metabolic changes that were measured in the lungs of HFD mice at 8 dpi may provide a snapshot of some of the altered dynamic metabolic processes occurring during the infection. We utilized the GeneGo Metacore systems biology software to uncover differentially altered metabolic pathways (Figure 4D). The most significantly altered pathway in the lungs of obese mice at 8 dpi was N-Acyltransferase metabolism ($p<0.0005$), as well as a number of fatty acid-related pathways and nucleotide metabolism pathways (Figure 4D). For metabolite comparisons, we primarily focused on differences between CD and HFD mice as we detected the greatest discrepancy in infection severity between these two groups. However, a complete list of differentially altered metabolites between CD, LFD and HFD mice as well as fold change and p-values are listed in Supplemental Table 1.

Obesity, independent of diet, increases pH1N1 mortality

HFD mice exhibited greater pH1N1 infection severity, alterations in inflammatory immune responses and diverse changes in lung metabolism during the infection. However, a limitation of utilizing a diet model of obesity is that differential outcomes between lean (CD or LFD) and HFD obese mice could be influenced by differences in the diets, potentially confounding the effects of obesity. Further, LFD mice display greater mortality compared with CD mice, suggesting that simply modulating the diet (without causing any nutritional deficiencies) can impact pH1N1 infection outcome, although not to the same extent as in HFD obese mice. Therefore, we included a genetic model of obesity to assess the impact of obesity on infection responses independent of dietary effects.

We utilized a genetic model of obesity in which excess adiposity is driven primarily by hyperphagia (all mice are fed a CD). It has previously been shown that *ob/ob* mice, a robust model of genetic obesity, are more susceptible to pH1N1 infection compared with wild type mice (10). However, utilization of the *ob/ob* mouse model has a number of limitations due to the global deficiency of leptin signaling. Leptin is critical for proper physiology and immunity, and leptin deficiency has been shown to impair host defenses, thus, confounding the immunomodulatory consequences of obesity (8). Therefore, we used a tissue-specific model, previously characterized by Ring et al., in which disruption of leptin signaling is limited to hypothalamic neurons (the primary site of leptin-mediated appetite control) (32) to further address the impact of obesity on pH1N1 immunity. These mice become rapidly obese and exhibit hyperinsulinemia, hyperglycemia and hyperleptinemia among other metabolic alterations characteristic of obesity (32).

Male (Figure 5A) and female (Figure 5B) $LepR^{H-/-}$ mice, lacking functional leptin signaling in hypothalamic neurons, rapidly gained excess body weight compared to lean $LepR^{Hfl/fl}$ and $LepR^{H+/-}$ mice. At 13–16 wks of age, $LepR^{H-/-}$, $LepR^{H+/-}$, and $LepR^{Hfl/fl}$ mice were infected with 5.8×10^2 $TCID_{50}$ pH1N1. Strikingly, obese male (Figure 5C) and

female LepR$^{H-/-}$ (Figure 5D) mice were significantly more susceptible to pH1N1 mortality compared with lean LepR$^{H+/-}$ and LepR$^{Hfl/fl}$ mice. Obese, LepR$^{H-/-}$, mice lost more absolute weight during the pH1N1 infection compared with both lean groups (Figure 5E/F). Obese male and female LepR$^{H-/-}$ mice displayed a lower percentage of body weight lost compared with lean mice, this is likely due to the greater pre-infection weight of LepR$^{H-/-}$ mice (Figure 5G/H). There was no significant difference detected in percent mortality between male and female LepR$^{H-/-}$ mice; therefore, for further analyses, male and female mice were combined. Additionally, the mortality curve from HFD mice was not significantly different from either male or female LepR$^{H-/-}$ mice (data not shown).

Obese LepR$^{H-/-}$ mice exhibit greater lung inflammatory responses and alterations in lung immune cell populations during pH1N1 infection

Given the elevated mortality in the LepR$^{H-/-}$ obese mice compared with lean controls, we next assessed pathological and immunological responses in the lungs of LepR$^{H-/-}$ mice. Figure 6A demonstrates that while LepR$^{H-/-}$ mice had significantly larger mesenteric white adipose depots (mWAT) and livers compared with lean LepR$^{Hfl/fl}$ mice, there were no differences in lung weight. Lung viral titers were then measured, and LepR$^{H-/-}$ did not exhibit differences in viral burden (Figure 6B). However, the obese LepR$^{H-/-}$ mice did have fewer infiltrating cells into the airways during the infection (Figure 6C), but exhibited a greater level of injury to the lung epithelium compared with lean LepR$^{Hfl/fl}$ mice at 8 dpi (Figure 6D). Gene expression of lung cytokines and chemokines also demonstrated that the genetically obese mice had greater pulmonary inflammation at 8 dpi (Figure 6E). LepR$^{H-/-}$ mice exhibited higher levels of IL-10, MCP-1 and KC at 8 dpi.

In the dietary model of obesity, HFD mice had fewer BAL macrophages and Tregs. Therefore, the distribution of these cells in LepR$^{Hfl/fl}$ and LepR$^{H-/-}$ mice was assessed at 4 and 8 dpi (Figure 6F–H). Similar to HFD obese mice, LepR$^{H-/-}$ mice had fewer BAL macrophages (Figure 6F). Additionally, LepR$^{H-/-}$ mice also had fewer CD4^{+} T cells, CD8^{+} T cells (data not shown), BAL Tregs and activated BAL Tregs (Figure 6G/H). Therefore, both HFD and LepR$^{H-/-}$ obese mice exhibit similar differences in BAL macrophage and Treg numbers during pH1N1 infection in comparison with lean controls.

Obese LepR$^{H-/-}$ mice exhibit distinct metabolic perturbations in lung tissue during pH1N1 infection

To enhance our analysis of the metabolic consequences of obesity during pH1N1 infection, the lungs of LepR$^{Hfl/fl}$ and LepR$^{H-/-}$ mice were harvested at 0 and 8 dpi and processed for metabolic profiling. In Figures 7A–B, the OPLS-DA plots demonstrate significant separation between lung samples from uninfected and infected LepR$^{Hfl/fl}$ and LepR$^{H-/-}$ mice. LepR$^{H-/-}$ mice exhibited alterations in a number of lipid metabolites at both 0 and 8 dpi. Additionally, few metabolites differentially affected by obesity at 0 dpi were also different at 8 dpi, indicating the recovered metabolic data at 8 dpi are specific to the consequences of obesity during pH1N1 infection, rather than caused by obesity alone. Of interest, a majority of metabolites different between LepR$^{Hfl/fl}$ and LepR$^{H-/-}$ mice, were lower in the lungs of LepR$^{H-/-}$ mice. A pathway enrichment analysis based on the 8 dpi lung metabolomes of LepR$^{Hfl/fl}$ and LepR$^{H-/-}$ mice was constructed. Similar to pathways

altered in the lungs of HFD mice, a number of the pathways altered in obese Lepr$^{H-/-}$ mice were related to nucleotide or fatty acid metabolism as well as amino acid metabolism (Figure 7C).

Metabolic profiling of urine can differentiate lean LepR$^{Hfl/fl}$ mice and obese LepR$^{H-/-}$ at an early pH1N1 infection time point

We have previously demonstrated that ^{1}H-nuclear magnetic resonance-based metabolic profiling of urine can distinguish lean and obese mice infected with a sublethal dose of influenza A/Puerto Rico/8/1934 (H1N1) (26). Urinary profiling is both informative and readily translatable given that urine reflects a wide range of physiological and pathophysiological processes and is easily obtained in clinical settings (compared with tissues). We therefore sought to extend our metabolic analysis to include profiling of urine from uninfected and pH1N1 infected LepR$^{Hfl/fl}$ and Lepr$^{H-/-}$ mice. During the infection, we chose to profile urinary samples at 2 dpi. This time point occurs prior to drastic weight loss or obvious signs of sickness, allowing utilization of metabolic profiling for identifying biomarkers that may be used to predict or explain mechanisms of greater severity in LepR$^{H-/-}$ obese mice. The PLS-DA plot in Figure 8A demonstrates that UPLC-MS profiling was able to successfully distinguish urine from LepR$^{Hfl/fl}$ and LepR$^{H-/-}$ mice at 0 and 2 dpi. A relatively large number of metabolites were detected at greater levels in the urine at 0 dpi in LepR$^{H-/-}$ mice (Figure 8B). At 2 dpi, several unique metabolites were altered by infection in obese mice such as L-Acetylcarnitine, phosphatidylcholine and 8 different amino acid-related metabolites (Figure 8C). Lastly, pathway analysis of urine metabolomes at 2 dpi, revealed alterations in pathways related to fatty acid, amino acid and histamine metabolism (Figure 8D). Although it is known that obesity is characterized by alterations in fatty acid metabolism, we show for the first time that changes in fatty acid metabolic pathways (and several other pathways) occur systemically in the urine and locally in the lung during a pH1N1 infection.

Discussion

Obesity is a global epidemic, and the consequences of excess adiposity are diverse and continue to mount (45). Following the emergence of the 2009 pH1N1 strain, obesity was reported to be an independent risk factor for greater pH1N1 (17, 37–40) and seasonal (46–48) influenza infection severity. In this study, we provide an in-depth analysis of the immunologic and metabolic complications associated with obesity during infection with the 2009 pH1N1 influenza. Previous studies in mice have shown that obesity alters lung wound healing and inflammatory responses during a pH1N1 infection (10), possibly due to hyperleptinemia (11). However, the complications of obesity are complex, and a number of other factors could be affecting pH1N1 immunity such as: hyperglycemia, hyperinsulinemia, oxidative stress, changes in the gut microbiome, and alterations in cellular and systemic metabolism (9). Therefore we sought to combine immunological assessments with metabolomics to provide a more global characterization of the metabolic consequences of obesity on pH1N1 infection.

One of several mechanisms in which HFD-induced obesity may result in greater pH1N1 severity is the impact of consuming a high fat diet. Altering dietary composition, even without inducing nutritional deficiencies, can have systemic metabolic consequences (49–51) and can affect antiviral immunity (52). One inherent limitation with a diet-induced obesity model, is a high fat diet will always differ from a lean control diet (e.g. saturated fatty acid content, carbohydrate content etc.), potentially confounding the implications of the impact of obesity. One goal of this investigation was to provide an in-depth analysis of the consequences of HFD-induced obesity in comparison with two different lean control groups to better assess dietary contributions. It has previously been demonstrated that LFDs high in sucrose can have metabolic consequences and can impact immune responses (53). Additionally, the CD differs in nearly every aspect from the purified LFD and HFDs (yet is still one of the most widely used control diets for obesity studies) (54). Several key differing components are amounts of phytoestrogens and dietary fiber. Chow diets are primarily derived from plant constituents, and therefore contain phytoestrogens as well as dietary fiber (54). Phytoestrogens have been shown to affect metabolism and behavior. Further, fiber can also impact metabolic health and modulate the gut microbiome (54, 55), and the purified LFD has no fiber (perhaps contributing to greater weight gain and a somewhat intermediate metabolic phenotype between CD mice and HFD mice as in Figure 1). These differing characteristics of the diets likely explain some of the differential responses observed between the three dietary groups (especially between LFD and CD mice).

Currently, three studies have demonstrated that diet-induced obese mice exhibit greater mortality to a primary pH1N1 infection (10, 11, 15). Two of these studies used a CD for the lean control group and a 45% or 60% kcal HFD for obese mice (10, 11), and one study used a 60% kcal HFD compared with a nutrient matched, purified, 10% kcal low fat diet (15). Although we found HFD mice were more susceptible compared with both lean groups, lean LFD mice exhibited greater mortality compared with lean CD mice. This demonstrates that modulating the diet alone, without inducing obesity, can increase pH1N1 severity, and it is possible there are synergistic effects of being obese and consuming a HFD. This outcome may have potential public health implications in that perhaps not only being obese increases risk for influenza severity, but the composition of the diet one chooses to eat could also impact severity as well.

Given the complications of diet-induced obesity models, a genetic model of obesity was also included in our analysis in attempt to better assess the immunological consequences of excess adiposity independent of dietary effects. Obese, male and female $LepR^{H-/-}$ mice were significantly more susceptible to pH1N1 mortality compared with lean control groups. *Ob/ob* mice lacking the hormone leptin are a commonly used model of genetically-induced obesity, in which lack of leptin satiety cues result in hyperphagia and obesity (56, 57). O'Brien et al. has previously demonstrated that *ob/ob* obese mice were more susceptible to pH1N1 mortality (10). Although this is informative and helps to address the complications of dietary models discussed above, a global deficiency of leptin signaling can cause physiologic and immunologic complications, confounding the effects of obesity (57). Therefore, we utilized a genetic model of obesity in which disruption of leptin signaling is isolated to hypothalamic neurons (although there is some evidence of Nkx2.1 expression in

the lungs, esophagus and during development (221)). This genetic model of obesity established that although diet may synergize with obesity to impact pH1N1 immunity, obesity alone is sufficient to increase pH1N1 mortality. Additionally, this study highlights the importance of careful consideration in choosing a mouse model of obesity (genetic- vs diet-induced), and in selecting proper dietary controls for HFD-induced obesity studies.

Both diet- and genetic-induced obese mice exhibited greater lung damage during the pH1N1 infection. This excess lung pathology has been demonstrated previously in obese mice, and is likely due to impaired wound healing in the lung (10). A number of potential mechanisms may be responsible for enhanced lung damage in obese mice. Tregs are critical regulators of immunopathology and have been shown to limit inflammatory responses to RSV and some influenza infection models in mice (41–43) We have previously demonstrated that obese mice have fewer Tregs in the lung airways during a secondary pH1N1 challenge, and Tregs isolated from obese mice exhibited impaired suppressive capacity compared with Tregs isolated from lean mice (14). Therefore, we also investigated the distribution of Tregs in the lung, lung airways and mLN during a primary pH1N1 infection. At 8 dpi, HFD- and genetic-induced obese mice had fewer BAL Tregs and fewer activated BAL Tregs. It is currently unclear why obese mice have fewer BAL Tregs during influenza infection, but it is well established that obesity results in a deficiency of Tregs in metabolic tissues such as the liver and white adipose tissue (8, 9). Obesity results in greater lung damage during both primary and secondary pH1N1 infections, and therefore uncovering how obesity modulates BAL Treg responses is likely important for understanding the complex mechanisms of influenza severity caused by an obese state.

Additionally, fewer F4/80^{+} macrophages were detected in the lung airways of obese mice at 4 dpi in HFD mice and at 8 dpi in LepR$^{H-/-}$ mice. NK cell numbers were also slightly lower in HFD mice compared with CD mice, but this did not reach statistical significance ($p=0.07$). Macrophages fulfill a diverse number of processes in infection recovery such as propagating inflammatory responses or promoting wound healing (16, 58). For example, alternatively activated macrophages are prototypically anti-inflammatory and facilitate wound healing (16). Although we did not phenotype BAL macrophages, perhaps obese mice had fewer BAL alternatively activated macrophages during infection, contributing to greater immunopathology. Future investigations are necessary to assess how obesity modulates macrophage polarization and function in the lung during pH1N1 infection.

Obesity is inherently a metabolic disease. Therefore, we hypothesized that metabolic profiling can be used to enhance our current understanding of the consequences of obesity on influenza infection. A partial least square discriminant analysis of the broad spectrum metabolomics data successfully distinguished lung samples on the basis of both obesity and infection status. In lung tissue from uninfected and infected HFD mice, several lipid species related to fatty acid, cholesterol or phospholipid metabolism were altered compared with CD mice. Of interest, the number of lipid metabolites altered in HFD lungs nearly tripled by 8 dpi, with some lipid metabolites such as 3-Oxododecanoic acid and 4-Hydroxyisovaleric acid detected at nearly 10-fold greater concentrations. Obesity is associated with greater levels of circulating unesterified fatty acids and TAG (8), but why these lipid metabolites are altered in the lungs of obese mice at 8 dpi (rather than in uninfected mice or at 4 dpi) is

unknown. Perhaps the complex milieu of excess inflammatory cytokines and metabolic hormones in the lungs of obese mice impacts cellular metabolism, ultimately impeding proper lung healing and recovery.

Metabolic profiling of lung tissue revealed several interesting findings. P-cresol sulfate was detected at a 5-fold greater concentration in uninfected HFD-obese mice compared with CD mice. By 4 dpi, p-cresol sulfate was detected at a 55-fold greater level in the lungs of HFD-obese mice, and remained elevated at 8 dpi with HFD mice showing greater than 10x p-cresol sulfate levels. P-cresol sulfate is a metabolite derived from secondary metabolism of p-cresol by gut microbiota, typically reported to be found in the urine (59). P-cresol sulfate accumulates during conditions of kidney failure, and some evidence indicates it may be toxic (59, 60) and can impact immune cell function (61). Although, we did not measure urinary p-cresol sulfate in HFD mice, perhaps elevated levels of this metabolite may reflect impaired kidney function. Additionally, given that P-cresol sulfate is a microbial derived metabolite, it is also possible that influenza differentially alters gut microbiota function in obese mice, ultimately impacting antiviral immune responses. It has previously been demonstrated that altering the gut microbiome can affect influenza infection immunity in mice (62). Of interest, LFD mice also exhibited greater concentrations of lung p-cresol sulfate compared with CD mice, suggesting that perhaps elevated p-cresol sulfate levels are due to dietary-microbiome interactions. There is little known regarding p-cresol sulfate in the lung or during the context of an infection, but the strikingly elevated levels detected in the lungs of HFD mice merit further investigation.

A number of other metabolites notably elevated in the lungs of HFD mice include glutamyl-proline (increased in HFD mice at 4 and 8 dpi), tetrahydrocotisol (4 dpi), 3-hydroxybutric acid (8 dpi) and the numerous acyl-carnitine species elevated at 8 dpi in HFD lungs. Chronic overnutrion is thought to increase cytosolic lipid content in insulin-sensitive tissues (such as liver and skeletal muscle), which can ultimately impair insulin signaling (63). Perhaps the elevated levels of acyl-carnitines reflect these processes in the lung. Further, accumulation of acyl-carnitines may indicate impaired fatty acid oxidation in lung cells (63). Taken together, the diverse changes in the lung metabolome of HFD mice during pH1N1 may reflect pathological processes contributing to greater infection severity.

$LepR^{H-/-}$ mice also exhibited alterations in an array of lung metabolites prior to and during the pH1N1 infection. One notable difference between HFD-obese mice and $LepR^{H-/-}$ obese mice was that most differentially altered metabolites in HFD mice were elevated compared to CD mice, whereas most metabolites in $LepR^{H-/-}$ mice were detected at a lower concentration compared with $LepR^{Hfl/fl}$ mice. Further, relatively few metabolites were similarly altered in both obesity models. At 8 dpi, only arachidonic acid and hydroxyvalerylcarnitine were elevated in the lungs of both HFD and $LepR^{H-/-}$ mice compared with lean controls. Of interest, arachidonic acid is a substrate for eicosanoid metabolism, and arachidonic acid metabolites (such as leukotrienes and prostaglandins) can impact inflammatory responses (64). The fact that the lung metabolomes in HFD and $LepR^{H-/-}$ mice differ greatly, highlights the impact of the diet in this model. Future studies are required to better understand the synergistic effects of a HFD and excess adiposity, and how these factors interact to modulate the lung metabolome and affect pH1N1 immunity.

We also performed metabolic profiling on urine samples from $LepR^{Hfl/fl}$ and $LepR^{H-/-}$ mice at 2 dpi. Similar to changes in lung metabolites, alterations in urinary metabolites related to fatty acid, nucleotide and amino acid metabolism were measured. The fact that metabolic profiling can distinguish $LepR^{H-/-}$ mice from lean control mice as early as 2 dpi (prior to any obvious signs of illness or drastic weight loss), introduces the possibility of utilizing metabolic profiling to compliment current prognostic or diagnostic approaches in the future. Additionally, the urinary metabolome may provide insight into the mechanisms in which obesity increases pH1N1 mortality. For example, taurine was elevated in the urine of obese $LepR^{H-/-}$ mice at 2 dpi. Detection of taurine has been reported to be increased under conditions of oxidative stress (65). The fold change of taurine increased from slightly greater in uninfected urine of $LepR^{H-/-}$ mice to 4-fold greater by 2 dpi. Therefore, this may indicate that influenza infection induces greater oxidative stress in obese mice.

Taken together, we have provided the first analysis of both the immunologic and metabolic consequences of obesity during pH1N1 infection. It is likely that the distinct metabolic perturbations detected in the lungs of obese mice are both reflective and inflictive of pathologic changes occurring in the lung following infection. In addition, we were able to document distinct changes in the urine of infected mice before overt signs of illness, demonstrating the strength of this approach. Future studies are required to further integrate this metabolomic data with immunologic responses to identify novel mechanisms for greater pH1N1 severity in obese mice.

Supplementary Material

Refer to Web version on PubMed Central for supplementary material.

Acknowledgments

This work was supported in part by NIH supported NORC DK56350, the Flight Attendants Medical Research Institute (FAMRI) (CIA-103071), and the metabolomics analysis was supported by the NIH Common Fund Metabolomics Program. The UNC Flow Cytometry Core Facility is supported in part by an NCI Center Core Support Grant (P30CA06086) to the UNC Lineberger Comprehensive Cancer Center.

Abbreviations used in this paper

AMPK	AMP-activated protein kinase
BAL	bronchoalveolar lavage
BALF	bronchoalveolar lavage fluid
BMI	body mass index
CD	chow diet
dpi	days post-infection
HFD	high fat diet
LFD	low fat diet
MDCK	Madin-Darby canine kidney cells

$LepR^{Hfl/fl}$	fully floxed leptin receptor mice
$LepR^{H+/-}$	heterozygous mice
$LepR^{H-/-}$	mice with disruption of leptin receptor signaling in hypothalamic neurons
NK cells	natural killer cells
UPLC-MS	ultra-performance liquid chromatography-mass spectrometry
mWAT	mesenteric white adipose tissue
mLN	mediastinal lymph nodes
OPLS-DA	orthogonal partial least square discriminant analysis
pH1N1	2009 pandemic H1N1 influenza A virus, A/California/04/2009
PLS-DA	partial least squares discriminant analysis
$TCID_{50}$	50% tissue culture infective dose
TAG	triacylglycerol
Treg	regulatory T-cell

References

1. Centers for Disease Control and Prevention. 2009 H1N1: Overview of a Pandemic. Dec. 2010 [cited 19 August 2014]http://www.cdc.gov/h1n1flu/yearinreview/yir1.html
2. World Health Organization. A (H1N1) seasonal influenza virus: guidance on prevention and treatment. Feb. 2014 [cited 19 August 2014]http://www.emro.who.int/egy/egypt-news/a-h1n1-is-a-seasonal-influenza-virus-guidance-on-prevention-and-treatment.html
3. Hanslik T, Boelle PY, Flahault A. Preliminary estimation of risk factors for admission to intensive care units and for death in patients infected with A (H1N1) 2009 influenza virus, France, 2009–2010. PLoS Currents. 2010; 2(RRN1150)
4. Louie JK, Acosta M, Samuel MC, Schechter R, Vugia DJ, Harriman K, Matyas BT. the California Pandemic (H1N1) Working Group . A Novel Risk Factor for a Novel Virus: Obesity and 2009 Pandemic Influenza A (H1N1). Clin Infect Dis. 2011; 52:301–312. [PubMed: 21208911]
5. Santa-Olalla Peralta P, Cortes-Garcia M, Vicente-Herrero M, Castrillo-Villamandos C, Arias-Bohigas P, Pachon-del Amo I, Sierra-Moros MJ. Surveillance Group for New Influenza A(H1N1) Virus Investigation and Control Team in Spain . Risk factors for disease severity among hospitalised patients with 2009 pandemic influenza A (H1N1) in Spain, April - December 2009. Euro Surveill. 2010; 15:19667. [PubMed: 20929651]
6. Morgan OW, Bramley A, Fowlkes A, Freedman DS, Taylor TH, Gargiullo P, Belay B, Jain S, Cox C, Kamimoto L. Morbid obesity as a risk factor for hospitalization and death due to 2009 pandemic influenza A (H1N1) disease. PLoS One. 2010; 5:e9694. [PubMed: 20300571]
7. World Health Organization. WHO Factsheet 311: Obesity and Overweight. May. 2012 [cited 2 August, 2012]http://www.who.int/mediacentre/factsheets/fs311/en/index.html
8. Milner JJ, Beck MA. The impact of obesity on the immune response to infection. Proc Nutr Soc. 2012; 71:298–306. [PubMed: 22414338]
9. Milner JJ, Beck MA. Obesity and influenza infection severity. Fut Virol. 2014; 9:223–225.
10. O'Brien KB, Vogel P, Duan S, Govorkova EA, Webby RJ, McCullers JA, Schultz-Cherry S. Impaired Wound Healing Predisposes Obese Mice to Severe Influenza Virus Infection. J Infect Dis. 2012; 205:252–261. [PubMed: 22147799]
11. Zhang AJ, To KK, Li C, Lau CC, Poon VK, Chan CC, Zheng B, Hung IF, Lam KS, Xu A. Leptin mediates the pathogenesis of severe 2009 pandemic influenza A (H1N1) infection associated with

cytokine dysregulation in mice with diet-induced obesity. J Infect Dis. 2013; 207:1270–1280. [PubMed: 23325916]

12. Karlsson EA, Sheridan PA, Beck MA. Diet-Induced Obesity Impairs the T Cell Memory Response to Influenza Virus Infection. J Immunol. 2010; 184:3127–3133. [PubMed: 20173021]
13. Kim YH, Kim JK, Kim DJ, Nam JH, Shim SM, Choi YK, Lee CH, Poo H. Diet-induced obesity dramatically reduces the efficacy of a 2009 pandemic H1N1 vaccine in a mouse model. J Infect Dis. 2012; 205:244–251. [PubMed: 22147801]
14. Milner J, Sheridan P, Karlsson E, Schultz-Cherry S, Shi Q, Beck M. Diet-induced obese mice exhibit altered heterologous immunity during a secondary 2009 pandemic H1N1 infection. J Immunol. 2013; 191:2474–2485. [PubMed: 23904168]
15. Easterbrook JD, Dunfee RL, Schwartzman LM, Jagger BW, Sandouk A, Kash JC, Memoli MJ, Taubenberger JK. Obese mice have increased morbidity and mortality compared to non-obese mice during infection with the 2009 pandemic H1N1 influenza virus. Influenza Other Respi Viruses. 2011; 5:418–425.
16. Johnson AR, Justin Milner J, Makowski L. The inflammation highway: metabolism accelerates inflammatory traffic in obesity. Immunol Rev. 2012; 249:218–238. [PubMed: 22889225]
17. Jain S, Kamimoto L, Bramley AM, Schmitz AM, Benoit SR, Louie J, Sugerman DE, Druckenmiller JK, Ritger KA, Chugh R. Hospitalized patients with 2009 H1N1 influenza in the United States, April–June 2009. N Engl J Med. 2009; 361:1935–1944. [PubMed: 19815859]
18. Van Kerkhove MD, Vandemaele KA, Shinde V, Jaramillo-Gutierrez G, Koukounari A, Donnelly CA, Carlino LO, Owen R, Paterson B, Pelletier L. Risk factors for severe outcomes following 2009 influenza A (H1N1) infection: a global pooled analysis. PLoS Medicine. 2011; 8:e1001053. [PubMed: 21750667]
19. Rizza S, Copetti M, Rossi C, Cianfarani M, Zucchelli M, Luzi A, Pecchioli C, Porzio O, Di Cola G, Urbani A. Metabolomics signature improves the prediction of cardiovascular events in elderly subjects. Atherosclerosis. 2014; 232:260–264. [PubMed: 24468136]
20. Abu-Hayyeh S, Williamson C. Estradiol, FXR and altered metabolism in pregnancy. Hepatology. 2014; 60:1815–1817. [PubMed: 24975680]
21. Shearer J, Duggan G, Weljie A, Hittel D, Wasserman D, Vogel H. Metabolomic profiling of dietary-induced insulin resistance in the high fat–fed C57BL/6J mouse. Diabetes Obes Metab. 2008; 10:950–958. [PubMed: 18215169]
22. Jung JY, Kim YN, Shin JH, Lee HS, Seong JK. 1H NMR-based metabolite profiling of diet-induced obesity in a mouse mode. BMB Rep. 2012; 45:419–424. [PubMed: 22831978]
23. Wang Y, Utzinger J, Saric J, Li JV, Burckhardt J, Dirnhofer S, Nicholson JK, Singer BH, Brun R, Holmes E. Global metabolic responses of mice to Trypanosoma brucei brucei infection. Proc Natl Acad Sci U S A. 2008; 105:6127–6132. [PubMed: 18413599]
24. Saric J, Li JV, Utzinger J, Wang Y, Keiser J, Dirnhofer S, Beckonert O, Sharabiani MT, Fonville JM, Nicholson JK. Systems parasitology: effects of Fasciola hepatica on the neurochemical profile in the rat brain. Mol Syst Biol. 2010; 6
25. Saric J, Li JV, Wang Y, Keiser J, Bundy JG, Holmes E, Utzinger J. Metabolic profiling of an Echinostoma caproni infection in the mouse for biomarker discovery. PLoS Negl Trop Dis. 2008; 2:e254. [PubMed: 18596973]
26. Milner JJ, Wang J, Sheridan PA, Ebbels T, Beck MA, Saric J. 1H NMR-Based Profiling Reveals Differential Immune-Metabolic Networks during Influenza Virus Infection in Obese Mice. PloS One. 2014; 9:e97238. [PubMed: 24844920]
27. Morita M, Kuba K, Ichikawa A, Nakayama M, Katahira J, Iwamoto R, Watanebe T, Sakabe S, Daidoji T, Nakamura S. The lipid mediator protectin D1 inhibits influenza virus replication and improves severe influenza. Cell. 2013; 153:112–125. [PubMed: 23477864]
28. Tam VC, Quehenberger O, Oshansky CM, Suen R, Armando AM, Treuting PM, Thomas PG, Dennis EA, Aderem A. Lipidomic profiling of influenza infection identifies mediators that induce and resolve inflammation. Cell. 2013; 154:213–227. [PubMed: 23827684]
29. Janke R, Genzel Y, Wetzel M, Reichl U. Effect of influenza virus infection on key metabolic enzyme activities in MDCK cells. BMC Proceedings. 2011; 5:129.

30. Ritter JB, Wahl AS, Freund S, Genzel Y, Reichl U. Metabolic effects of influenza virus infection in cultured animal cells: Intra- and extracellular metabolite profiling. BMC Syst Biol. 2010; 4:61. [PubMed: 20465796]

31. Chen L, Fan J, Li Y, Shi X, Ju D, Yan Q, Yan X, Han L, Zhu H. Modified Jiu Wei Qiang Huo decoction improves dysfunctional metabolomics in influenza A pneumonia-infected mice. Biomed Chromatogr. 2013; 28:468–474. [PubMed: 24132661]

32. Ring LE, Zeltser LM. Disruption of hypothalamic leptin signaling in mice leads to early-onset obesity, but physiological adaptations in mature animals stabilize adiposity levels. J Clin Invest. 2010; 120:2931–2941. [PubMed: 20592471]

33. Reed LJ, Muench H. A simple method of estimating fifty per cent endpoints. Am J Epidemiol. 1938; 27:493–497.

34. Dunn WB, Broadhurst D, Begley P, Zelena E, Francis-McIntyre S, Anderson N, Brown M, Knowles JD, Halsall A, Haselden JN. Procedures for large-scale metabolic profiling of serum and plasma using gas chromatography and liquid chromatography coupled to mass spectrometry. Nature Protocols. 2011; 6:1060–1083.

35. Trygg J, Holmes E, Lundstedt T. Chemometrics in metabonomics. J Proteome Res. 2007; 6:469–479. [PubMed: 17269704]

36. Smith AG, Sheridan PA, Harp JB, Beck MA. Diet-induced obese mice have increased mortality and altered immune responses when infected with influenza virus. J Nutr. 2007; 137:1236–1243. [PubMed: 17449587]

37. Intensive-care patients with severe novel influenza A (H1N1) virus infection-Michigan, June 2009. Morb Mortal Wkly Rep. 2009; 58:749–752.

38. Louie JK, Acosta M, Samuel MC, Schechter R, Vugia DJ, Harriman K, Matyas BT. A novel risk factor for a novel virus: obesity and 2009 pandemic influenza A (H1N1). Clin Infect Dis. 2011; 52:301–312. [PubMed: 21208911]

39. Morgan OW, Bramley A, Fowlkes A, Freedman DS, Taylor TH, Gargiullo P, Belay B, Jain S, Cox C, Kamimoto L. Morbid obesity as a risk factor for hospitalization and death due to 2009 pandemic influenza A (H1N1) disease. PLoS One. 2010; 5:e9694. [PubMed: 20300571]

40. Ren Y, Yin Y, Li W, Lin Y, Liu T, Wang S, Zhang S, Li Z, Wang X, Bi Z. Risk factors associated with severe manifestations of 2009 pandemic influenza A (H1N1) infection in China: a case--control study. Virol J. 2013; 10:149. [PubMed: 23672278]

41. Bedoya F, Cheng GS, Leibow A, Zakhary N, Weissler K, Garcia V, Aitken M, Kropf E, Garlick DS, Wherry EJ, Erikson J, Caton AJ. Viral antigen induces differentiation of Foxp3+ natural regulatory T cells in influenza virus-infected mice. J Immunol. 2013; 190:6115–6125. [PubMed: 23667113]

42. Lee DCP, Harker JAE, Tregoning JS, Atabani SF, Johansson C, Schwarze J, Openshaw PJM. CD25+ Natural Regulatory T Cells Are Critical in Limiting Innate and Adaptive Immunity and Resolving Disease following Respiratory Syncytial Virus Infection. J Virol. Sep 1.2010 84:8790–8798. [PubMed: 20573822]

43. Fulton RB, Meyerholz DK, Varga SM. Foxp3+ CD4 Regulatory T Cells Limit Pulmonary Immunopathology by Modulating the CD8 T Cell Response during Respiratory Syncytial Virus Infection. J Immunol. 2010; 185:2382–2392. [PubMed: 20639494]

44. Betts RJ, Prabhu N, Ho AWS, Lew FC, Hutchinson PE, Rotzschke O, Macary PA, Kemeny DM. Influenza A Virus Infection Results in a Robust, Antigen-Responsive, and Widely Disseminated Foxp3 Regulatory T Cell Response. J Virol. 2012; 86:2817–2825. [PubMed: 22205730]

45. Caballero B. The global epidemic of obesity: an overview. Epidemiol Rev. 2007; 29:1–5. [PubMed: 17569676]

46. Kwong JC, Campitelli MA, Rosella LC. Obesity and respiratory hospitalizations during influenza seasons in Ontario, Canada: a cohort study. Clin Infect Dis. 2011; 53:413–421. [PubMed: 21844024]

47. Campitelli M, Rosella L, Kwong J. The association between obesity and outpatient visits for acute respiratory infections in Ontario, Canada. Int J Obes. 2013

48. Mertz D, Kim TH, Johnstone J, Lam P, Kuster SP, Fadel SA, Tran D, Fernandez E, Bhatnagar N, Loeb M. Populations at risk for severe or complicated influenza illness: systematic review and meta-analysis. BMJ. 2013; 347:f5061. [PubMed: 23974637]
49. Garg A, Bonanome A, Grundy SM, Zhang Z, Unger RH. Comparison of a high-carbohydrate diet with a high-monounsaturated-fat diet in patients with non-insulin-dependent diabetes mellitus. N Engl J Med. 1988; 319:829–834. [PubMed: 3045553]
50. Teague H, Fhaner CJ, Harris M, Duriancik DM, Reid GE, Shaikh SR. n-3 PUFAs enhance the frequency of murine B-cell subsets and restore the impairment of antibody production to a T-independent antigen in obesity. J Lipid Res. 2013; 54:3130–3138. [PubMed: 23986558]
51. Sumiyoshi M, Sakanaka M, Kimura Y. Chronic intake of high-fat and high-sucrose diets differentially affects glucose intolerance in mice. J Nutr. 2006; 136:582–587. [PubMed: 16484528]
52. Schwerbrock NM, Karlsson EA, Shi Q, Sheridan PA, Beck MA. Fish oil-fed mice have impaired resistance to influenza infection. J Nutr. 2009; 139:1588–1594. [PubMed: 19549756]
53. Li Z, Soloski MJ, Diehl AM. Dietary factors alter hepatic innate immune system in mice with nonalcoholic fatty liver disease. Hepatology. 2005; 42:880–885. [PubMed: 16175608]
54. Warden CCH. Comparisons of Diets Used in Animal Models of High-Fat Feeding. Cell Metabolism. 2008; 7:277. [PubMed: 18396128]
55. Kuo SM. The interplay between fiber and the intestinal microbiome in the inflammatory response. Adv Nutr. 2013; 4:16–28. [PubMed: 23319119]
56. Klebanov S, Astle CM, DeSimone O, Ablamunits V, Harrison DE. Adipose tissue transplantation protects ob/ob mice from obesity, normalizes insulin sensitivity and restores fertility. J Endocrinol. 2005; 186:203–211. [PubMed: 16002549]
57. Kennedy AJ, Ellacott KL, King VL, Hasty AH. Mouse models of the metabolic syndrome. Dis Model Mech. 2010; 3:156–166. [PubMed: 20212084]
58. Lee SM, Dutry I, Peiris JS. Editorial: macrophage heterogeneity and responses to influenza virus infection. J Leukoc Biol. 2012; 92:1–4. [PubMed: 22745457]
59. Patel KP, Luo FJ, Plummer NS, Hostetter TH, Meyer TW. The production of p-cresol sulfate and indoxyl sulfate in vegetarians versus omnivores. Clin J Am Soc Nephrol. 2012; 7:982–988. [PubMed: 22490877]
60. Vanholder R, Bammens B, de Loor H, Glorieux G, Meijers B, Schepers E, Massy Z, Evenepoel P. Warning: the unfortunate end of p-cresol as a uraemic toxin. Nephrol Dial Transplant. 2011; 26:1464–1467. [PubMed: 21406546]
61. Schepers E, Meert N, Glorieux G, Goeman J, Van der Eycken J, Vanholder R. P-cresylsulphate, the main in vivo metabolite of p-cresol, activates leucocyte free radical production. Nephrol Dial Transplant. 2007; 22:592–596. [PubMed: 17040995]
62. Ichinohe T, Pang IK, Kumamoto Y, Peaper DR, Ho JH, Murray TS, Iwasaki A. Microbiota regulates immune defense against respiratory tract influenza A virus infection. Proc Natl Acad Sci USA. 2011; 108:5354–5359. [PubMed: 21402903]
63. Schooneman MG, Vaz FM, Houten SM, Soeters MR. Acylcarnitines: reflecting or inflicting insulin resistance? Diabetes. 2013; 62:1–8. [PubMed: 23258903]
64. Mancuso P, Peters-Golden M, Goel D, Goldberg J, Brock TG, Greenwald-Yarnell M, Myers MG Jr. Disruption of leptin receptor-STAT3 signaling enhances leukotriene production and pulmonary host defense against pneumococcal pneumonia. J Immunol. 2011; 186:1081–1090. [PubMed: 21148797]
65. Marcinkiewicz J, Kontny E. Taurine and inflammatory diseases. Amino Acids. 2014; 46:7–20. [PubMed: 22810731]

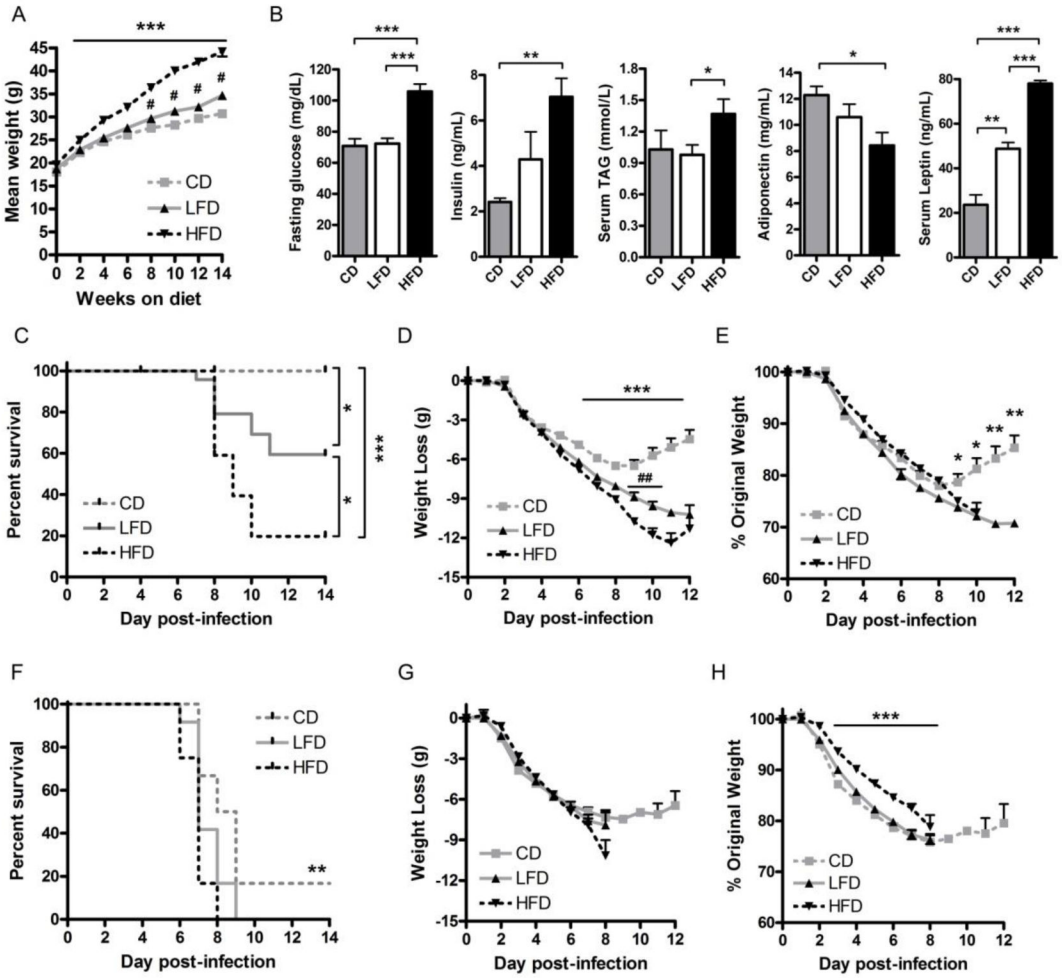

Figure 1.

HFD-induced obesity increases pH1N1 morbidity and mortality. A, Weanling, male, C57BL6/J mice were randomly placed on a high fat (HFD, 60% kcal fat), low fat (LFD, 10% kcal fat) or chow diet (CD 14% kcal fat) for 14 wks (n>30). B, Mice were fasted overnight and blood glucose was measured (n=8) as well as non-fasted serum insulin, TAG, adiponectin, and leptin (n=6–7). C, After 14–16 wks of dietary exposure, mice were infected intranasally with 5.8×10^2 $TCID_{50}$ pH1N1 and monitored for death (n≥21). D/E, Absolute weight loss (D) and percent weight loss (E) normalized to day 0, pre-infection weight over the course of the pH1N1 infection (n≥21). F, After 14–15 wks of dietary exposure, mice were infected with 1.3×10^3 $TCID_{50}$ and mortality was monitored (n=12). G/H, Absolute weight loss (G) and percent weight loss normalized to day 0, pre-infection weight (H) over the course of the 1.3×10^3 $TCID_{50}$ pH1N1 infection (n=12). Each bar or data point represents mean ± SEM. *p<0.05, **p<0.005, ***p<0.0005 comparing HFD with LFD and CD mice, and #p<0.05 ##p<0.005 comparing LFD and HFD mice.

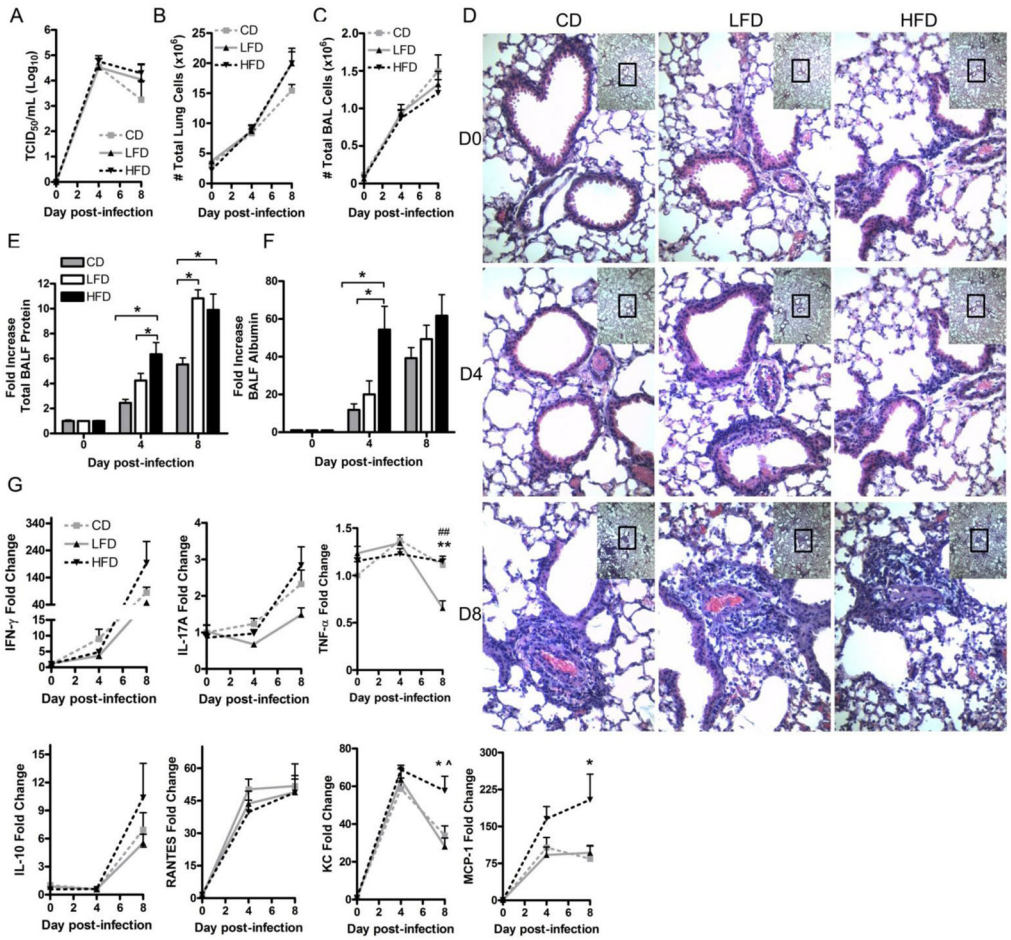

Figure 2.

HFD mice exhibit greater pH1N1 lung damage and inflammation. A, BALF viral titers after 5.8×10^2 $TCID_{50}$ pH1N1 infection (n=4 for uninfected mice and n=7–8 at 4 and 8 dpi). B/C, Total number of BAL cells (B) and lung cells (C, n≥8). D, H&E stained lung pathology slides (n=6–8). Each pathology image represents a 40x magnification of the designated area shown in the 4x magnified image in the top right of each field. E/F, Fold increase of BALF protein (E, n=6–10) and BALF albumin (F, n=5–7) during the pH1N1 infection. Fold increase normalized to uninfected mice within each dietary group. G, Fold change of BALF cytokine concentrations between CD, LFD and HFD mice determined from a multiplex assay (n=5–8). Each bar or data point represents mean ± SEM. *p<0.05, **p<0.005 comparing HFD with CD mice, ^p<0.05 comparing HFD with LFD mice, and #p<0.05 comparing CD with LFD mice.

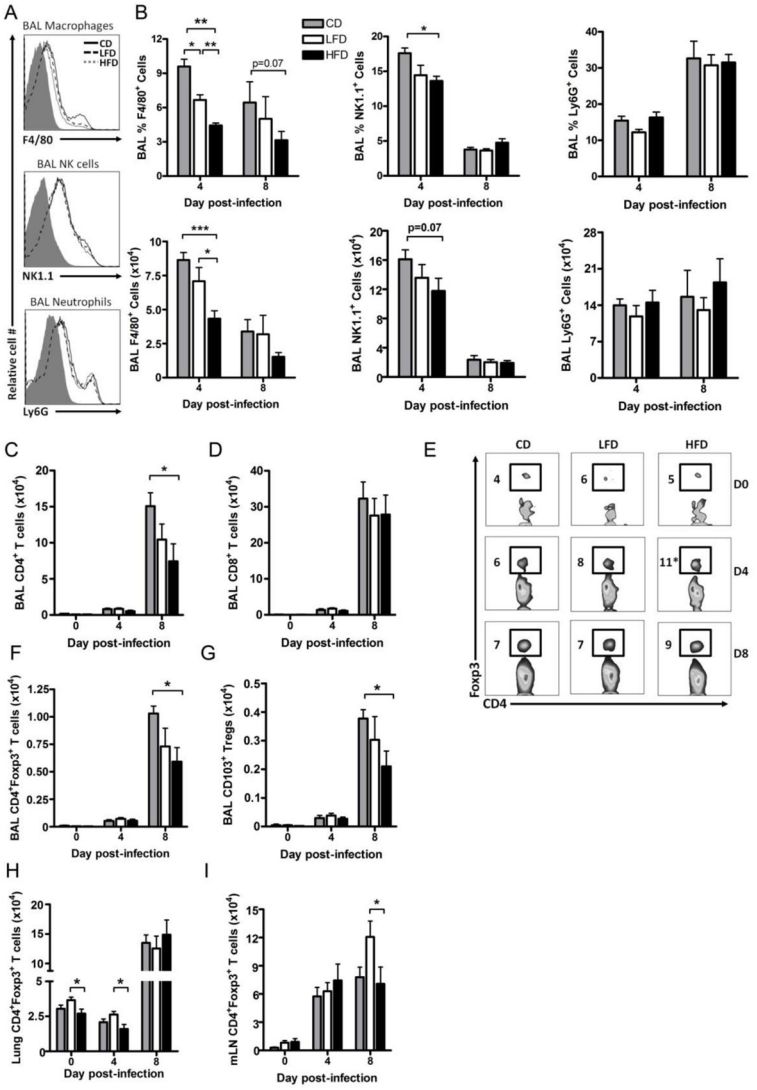

Figure 3.

HFD-induced obese mice have fewer BAL macrophages and Tregs during pH1N1 infection. A, Representative flow cytometry histograms of BAL macrophages, NK cells and neutrophils of CD, LFD and HFD mice at 4 dpi following a 5.8×10^2 $TCID_{50}$ pH1N1 infection. Fluorescence minus one (FMO) staining controls are shaded solid grey. B, Percentage (top) and total number (bottom) of BAL $F4/80^+$ cells, $NK1.1^+$ cells and $Ly6G^+$ cells (n=5–8). Percentage represents of total $CD3^{neg}$ cells. C–D, Number of BAL $CD4^+$ (C) and $CD8^+$ T cells (D). E, Representative Treg flow cytometry gating scheme. F–G, Number of BAL Tregs (F) and activated Tregs (G). H–I, Number of Lung Tregs (H) and mLN Tregs (I). For BAL cells n=3 of two pooled mice at day 0 and n=5–8 at 4 and 8 dpi. For mLN and lung cells, n=5–10. Each bar represents mean ± SEM. *p<0.05, **p<0.005, ***p<0.0005.

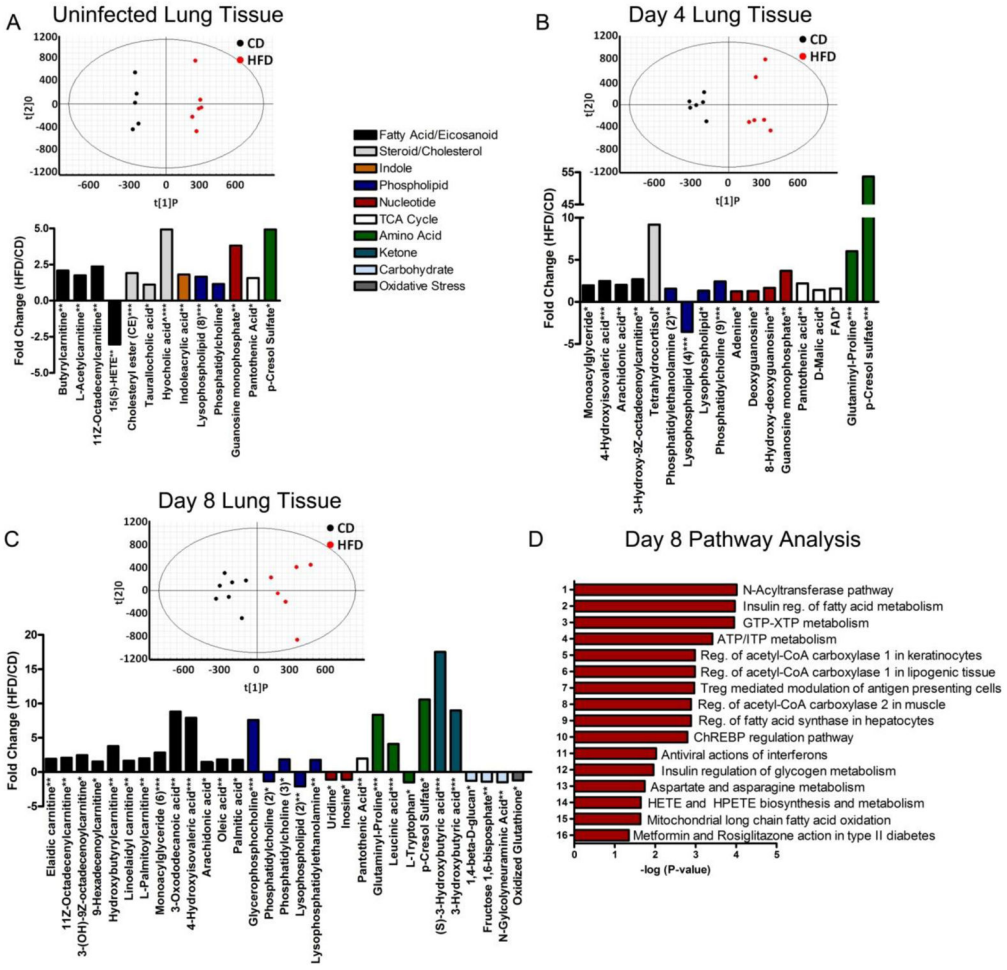

Figure 4.

HFD-induced obesity alters lung metabolic pathways during pH1N1 infection. A–C, OPLS-DA plot and differentially altered metabolites of lung samples from uninfected (A), 4 dpi (B) and 8 dpi (C) CD and HFD mice (n=5–6). Next to each metabolite, *p<0.05, **p<0.005, ***p<0.0005, and numbers in parentheses represent the number of species for that metabolite that are significantly different between HFD and LFD (i.e. methodology was not able to differentiate the multiple species). D, Pathway enrichment analysis generated in GeneGo of metabolic pathways significantly different between CD and HFD mice at 8 dpi. ChREBP, carbohydrate-responsive element-binding protein; HETE, hydroxyeicosatetraenoic acid; HPETE, hydroperoxyeicosatetraenoic acid.

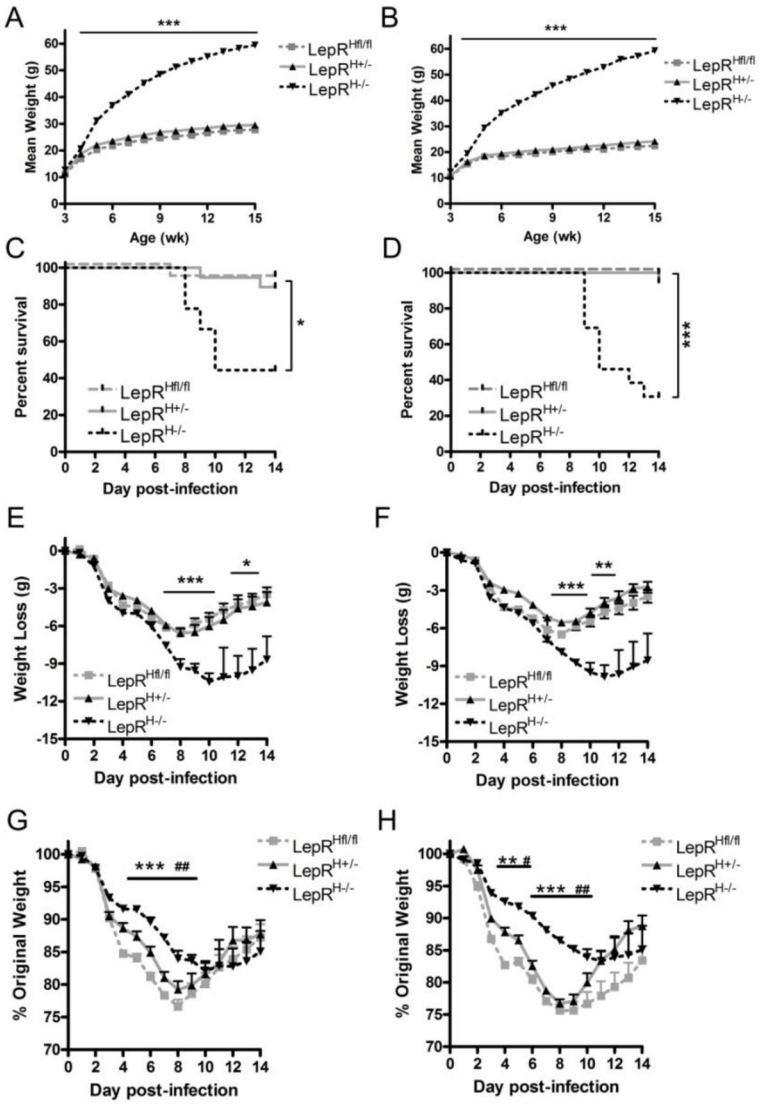

Figure 5.

Genetically obese, $LepR^{H-/-}$ mice, are more susceptible to pH1N1 mortality compared with lean $LepR^{Hfl/fl}$ mice. A–B, Weight gain of male (A) and female (B) mice lacking leptin receptor signaling in hypothalamic neurons $LepR^{H-/-}$, heterozygous mice $LepR^{H+/-}$ and fully floxed $LepR^{Hfl/fl}$ mice (n≥9). C–D, Mortality curves for male (C) and female (D) mice after infection with 5.8×10^2 $TCID_{50}$ pH1N1 at 14–16 wk of age (n≥9). E–F, Total weight loss for male (E) and female (F) mice after pH1N1 infection (n≥9). G–H, Percent weight loss for male (G) and female (H) mice after pH1N1 infection (n≥9. Each data point represents mean ± SEM. *p<0.05, **p<0.005, ***p<0.0005. In Figures A–F, *p<0.05, **p<0.005 or ***p<0.0005 comparing $LepR^{H-/-}$ with both $LepR^{H-/-}$ and $LepR^{H+/-}$ mice. For Figures G–H, **p<0.05 or ***p<0.0005 comparing $LepR^{H-/-}$ with $LepR^{Hfl/fl}$ mice and #p<0.05 or ##p<0.005 comparing $LepR^{H-/-}$ with $LepR^{H+/-}$ mice.

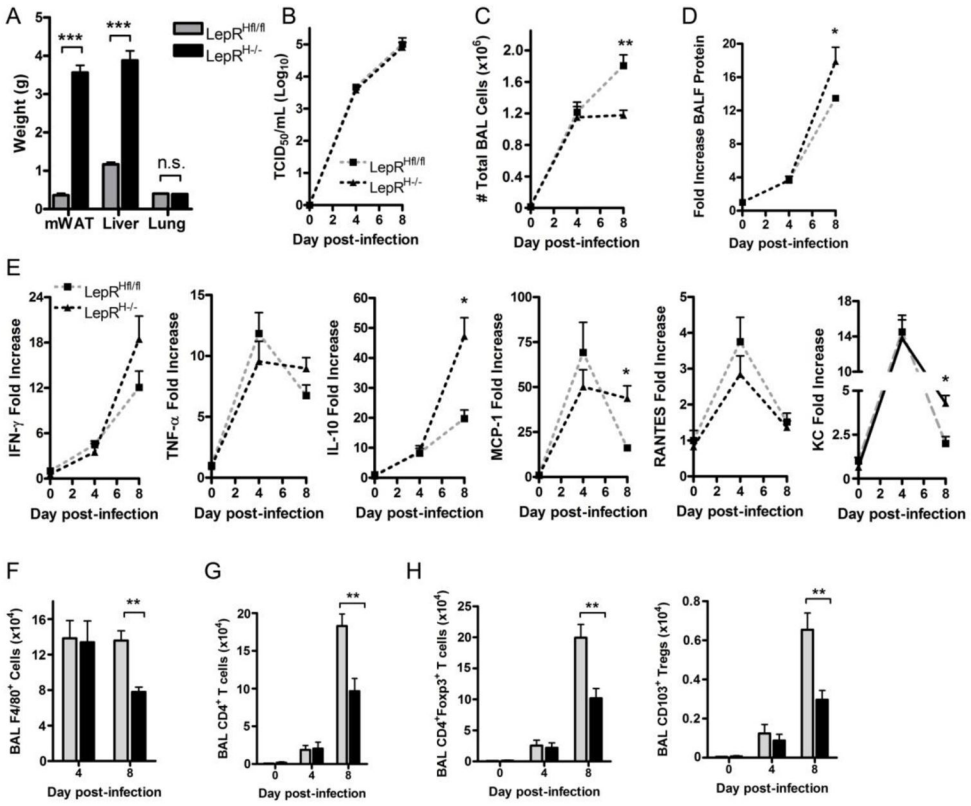

Figure 6.

Obese LepR$^{H-/-}$ mice exhibit greater pH1N1 lung damage and inflammation. A, Mean weight of mesenteric white adipose tissue, liver and lungs of LepR$^{Hfl/fl}$ and LepR$^{H-/-}$ mice prior to infection (n=7–10). B, BALF viral titers following a 5.8×10^2 $TCID_{50}$ pH1N1 infection (n=5–8). C, Total number of BAL cells during infection (at 0 dpi, n=4–5 from two pooled samples and at 4 and 8 dpi, n= 6–7). D, Fold increase in total BALF protein levels. Fold increase normalized to uninfected mice within each dietary group (n=6–8). E, Fold change in gene expression of lung cytokines and chemokines (n=4–6). F–H, Number of BAL $CD3^-F4/80^+$ macrophages (F), $CD4^+$ T cells (G), Tregs and activated Tregs (H, at 0 dpi, n=4–5 from two pooled samples and at 4/8 dpi, n= 6–7). Each bar represents mean ± SEM. *p<0.05, **p<0.005, ***p<0.0005.

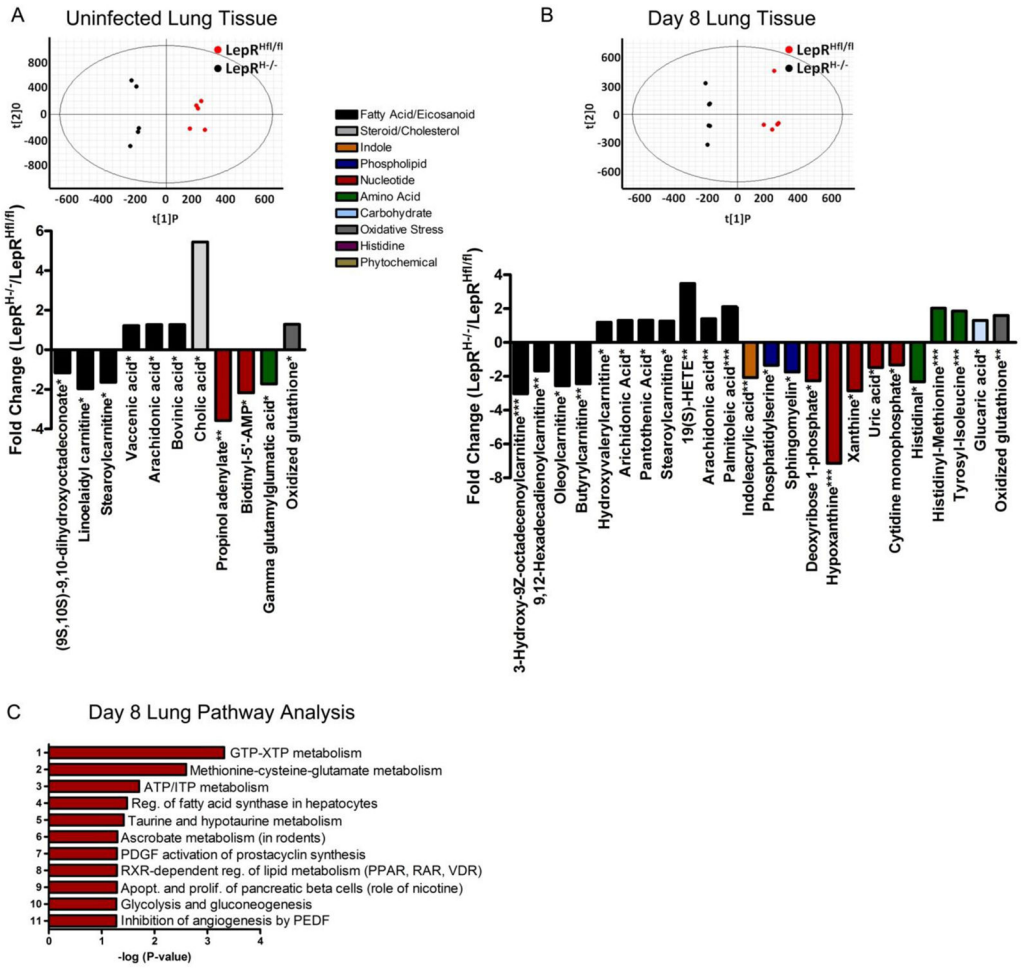

Figure 7.

Metabolic profiling reveals alterations in distinct metabolic networks in lungs of pH1N1 infected $LepR^{H-/-}$ obese mice. A–B, OPLS-DA plot and differentially altered metabolites of lung samples from uninfected (A) and 8 dpi (B) $LepR^{Hfl/fl}$ and $LepR^{H-/-}$ mice (n=5–6). C, Pathway analysis generated in GeneGo of all pathways significantly different from lung tissue of $LepR^{Hfl/fl}$ and $LepR^{H-/-}$ mice at 8 dpi. Next to each metabolite, *p<0.05, **p<0.005, ***p<0.0005. PDGF, platelet-derived growth factor; RXR, retinoid X receptor; PPAR, peroxisome proliferator-activated receptor; RAR, retinoic acid receptor; VDR, vitamin D receptor; PEDF, pigment epithelium-derived factor.

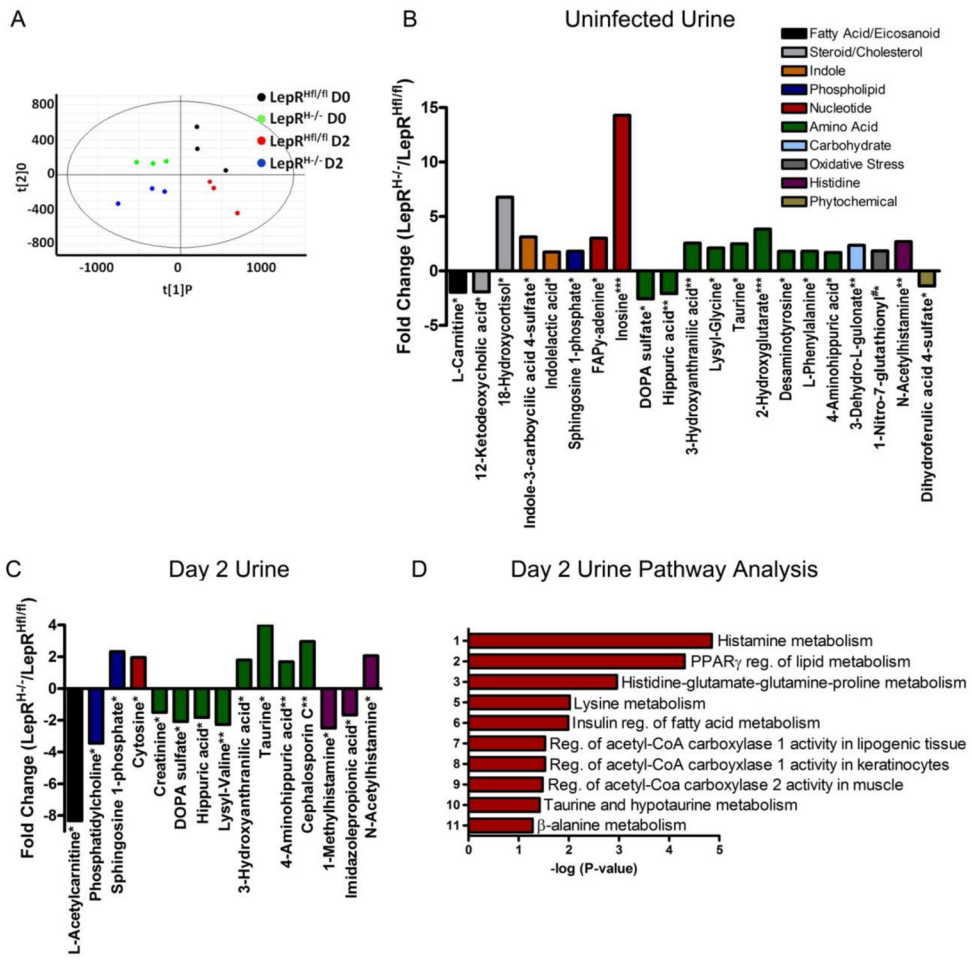

Figure 8.

Metabolic profiling reveals alterations in distinct metabolic networks in urine of pH1N1 infected obese LepR$^{H-/-}$ mice. A, OPLS-DA plot from urine samples from the same cohort of uninfected and 2 dpi infected mice. B–C, Differentially altered metabolites in the urine of uninfected (B) and at 2 dpi (C) LepR$^{H-/-}$ mice compared with lean LepR$^{Hfl/fl}$ mice (n=3). D, Pathway analysis generated in GeneGo of all pathways significantly different at 2 dpi between LepR$^{Hfl/fl}$ and LepR$^{H-/-}$ mice. Next to each metabolite, *p<0.05, **p<0.005, ***p<0.0005. # represents 1-Nitro-7-glutathionyl-8-hydroxy-7,8-dihydronapthalene. PPARγ, peroxisome proliferator-activated receptor γ.